Sustainable Energy & Fuels

ROYAL SOCIETY OF CHEMISTRY

PAPER

View Article Online
View Journal

Cite this: DOI: 10.1039/d6se00053c

Thermally controlled dual stabilization mechanisms of modified kenaf-derived lignin-based aqueous binders for silicon electrodes used in lithium-ion batteries

Tatsuki Hozumi,[a] Reiichi Chiba,[a] Masanori Ikeda,[a] Daisuke Tashima,[b] Yusuke Abe,[c] Seiji Kumagai *[c] and Takuya Egcuhi *[a]

Silicon (Si) is a promising anode material for lithium-ion batteries due to its high lithium storage capacity; however, severe volume expansion during charge–discharge cycling causes electrode degradation and rapid capacity fading. While binders are essential for maintaining electrode integrity, high-performance binders are often costly, complex to process, and dependent on organic solvents. Aqueous binders derived from natural polymers therefore represent attractive alternatives in terms of cost, sustainability, and environmental compatibility. Although chemically modified lignin binders are promising for Si electrodes, previous studies have only suggested the existence of two distinct thermal treatment approaches—low- and high-temperature processing—and no study has systematically compared these two methods. Herein, we report a modified kenaf-derived lignin copolymerized with polyacrylamide (KL-PAM) as an aqueous binder for Si electrodes and systematically investigate the effect of thermal treatment temperature on its stabilization mechanisms. Low-temperature-treated KL-PAM electrodes at 200 °C accommodated Si volume expansion through binder flexibility and adhesion, whereas high-temperature-treated electrodes were stabilized by carbonization-induced hardening of KL-PAM, which also enhanced electronic conductivity. As a result, high-temperature-treated electrodes at 600 °C exhibited superior rate capability, while capacity retention was comparable between the two regimes. Intermediate-temperature treatment was ineffective, leading to binder failure. This study clarifies thermally controlled dual stabilization mechanisms of lignin-based binders and provides guidance for the development of sustainable binders for Si electrodes in lithium-ion batteries.

Received 15th January 2026
Accepted 9th March 2026

DOI: 10.1039/d6se00053c

rsc.li/sustainable-energy

Introduction

Silicon (Si) has attracted attention as an anode active material for lithium-ion batteries and lithium-ion capacitors. Although Si offers a lithium storage capacity approximately ten times higher than that of conventional carbon-based anodes, it undergoes a large volume expansion of >300% during lithium-ion insertion and extraction.[1–4] This severe volume change causes pulverization of the Si active material and detachment of Si particles from the current collector, leading to rapid capacity fading and accelerated cycle degradation in energy storage devices. In electrodes, binders play a crucial role in bonding active material particles and fixing them to the current collector, and conventional binders such as poly(vinylidene fluoride) (PVDF), carboxymethyl cellulose (CMC), and styrene-butadiene rubber (SBR)/CMC have been widely used.[5–9] With the emergence of Si anodes, the development of high-performance binders possessing superior mechanical properties,[10–12] intrinsic electrical conductivity,[13,14] and even self-healing capability[15] has been actively pursued. However, improvements in binder performance are often accompanied by increased process complexity and the use of expensive polymeric materials, resulting in higher electrode manufacturing costs. In addition, increasingly stringent regulations on the use of organic solvents such as *N*-methyl-2-pyrrolidone (NMP) in binder preparation and electrode fabrication impose stricter equipment requirements, resulting in increased production costs.[7,8,16]

However, aqueous binders derived from modified polymers based on natural resources offer advantages in terms of resource availability, manufacturing cost, and environmental impact. Accordingly, various aqueous binders employing modified cellulose, gums, and alginates have been

[a]Department of Electrical and Electronic Engineering, College of Engineering, Nihon University, Koriyama 963-8642, Japan
[b]Department of Electrical Engineering, Graduate School of Engineering, Fukuoka Institute of Technology, 3-30-1, Japan
[c]Department of Mathematical Science and Electrical-Electronic-Computer Engineering, Graduate School of Engineering Science, Akita University, 1-1 Tegatagakuen-machi, Akita 010-8502, Japan. E-mail: kumagai@gipc.akita-u.ac.jp

reported.[6,7,17–19] Lignin is the second most abundant natural polymer after cellulose and functions as a natural binder in plant structures;[20] however, its application as a binder for battery electrodes has been scarcely reported.[21] Although unmodified lignin has been reported to provide binder performance comparable to that of conventional binders in lithium-ion batteries,[22,23] its application to Si-based electrodes requires enhanced mechanical properties.

Modified lignin binders produced *via* chemical polymerization exhibit superior binding properties compared to unmodified lignin owing to copolymerization, and various functionalities have been incorporated into these binders.[24–28] For instance, Luo *et al.* developed a lignin-*graft*-sodium polyacrylate modified lignin through a multistep synthesis process and applied it as a binder for Si electrodes, achieving a capacity retention of 91% after 100 cycles.[24] In these reports, the heat-treatment temperature during electrode fabrication was 100–110 °C, which falls within the conventional electrode processing range. Cheng *et al.* carbonized a polyethylene oxide-modified lignin binder in Si electrodes by heat treatment at 800 °C, enhancing mechanical strength and electronic conductivity;[29] a subsequent study identified 600 °C as optimal, delivering 2378 mAh g^{-1} after 100 cycles.[30] These studies indicate the existence of two distinct thermal-treatment approaches in the development of modified lignin-based binders, namely low-temperature and high-temperature treatments. However, no systematic study has yet directly compared these approaches or clearly elucidated the challenges and stabilization mechanisms specific to each thermal treatment method.

Herein, we aim to develop an aqueous lignin-derived binder and report a modified kenaf-derived lignin (KL-PAM) synthesized *via* copolymerization with polyacrylamide (PAM). Owing to its water solubility, PAM enables binder preparation and electrode fabrication using aqueous processing. Modified lignins copolymerized with PAM have been actively studied in various fields, including structural materials, hydrogels, and paper strength additives, and are known to exhibit high mechanical strength and excellent thermal stability.[31–39] Kenaf is a fast-growing plant whose cellulose is widely utilized for industrial applications, making its lignin a sustainable and underutilized resource.[40–42] In this study, by controlling the thermal treatment during electrode fabrication, we reveal dual stabilization mechanisms of Si electrodes enabled by KL-PAM binders. Furthermore, this study highlights the challenges associated with low- and high-temperature thermal treatments, providing insights into the development pathways of modified lignin-based binders.

Results and discussion

KL-PAM is synthesized following the procedure illustrated in Fig. 1(a). In this study, kenaf-derived lignin (KL) extracted *via* a conventional soda pulping process using an alkaline aqueous solution was employed as the starting material. The extracted KL was pulverized and dispersed in an aqueous KOH solution, after which PAM was added at a weight ratio of KL : PAM = 10 : 1 and stirred to obtain KL-PAM. Detailed information is provided in the SI. Thermogravimetric analysis under a nitrogen atmosphere was conducted to clarify the thermal decomposition temperatures of KL and KL-PAM, and the corresponding thermogravimetry (TG) and differential thermogravimetry (DTG) curves were obtained (Fig. 1(b)). Below 100 °C, dehydration and the removal of low-molecular-weight volatile species occur in lignin.[43] Between 200 and 350 °C, decomposition of carbohydrate components takes place, accompanied by the evolution of volatile gases.[44] Above 400 °C, the aromatic structures in lignin undergo decomposition or condensation, ultimately leading to the formation of carbonaceous residues.[44] The DTG curve of KL exhibited a main peak at 268 °C, followed by only a minor mass change above 600 °C, with a residual mass of 35.9% at 600 °C. In contrast, the DTG curve of KL-PAM shows a sharp peak at 229 °C and a broad peak centered at 413 °C in the range of 200–500 °C.

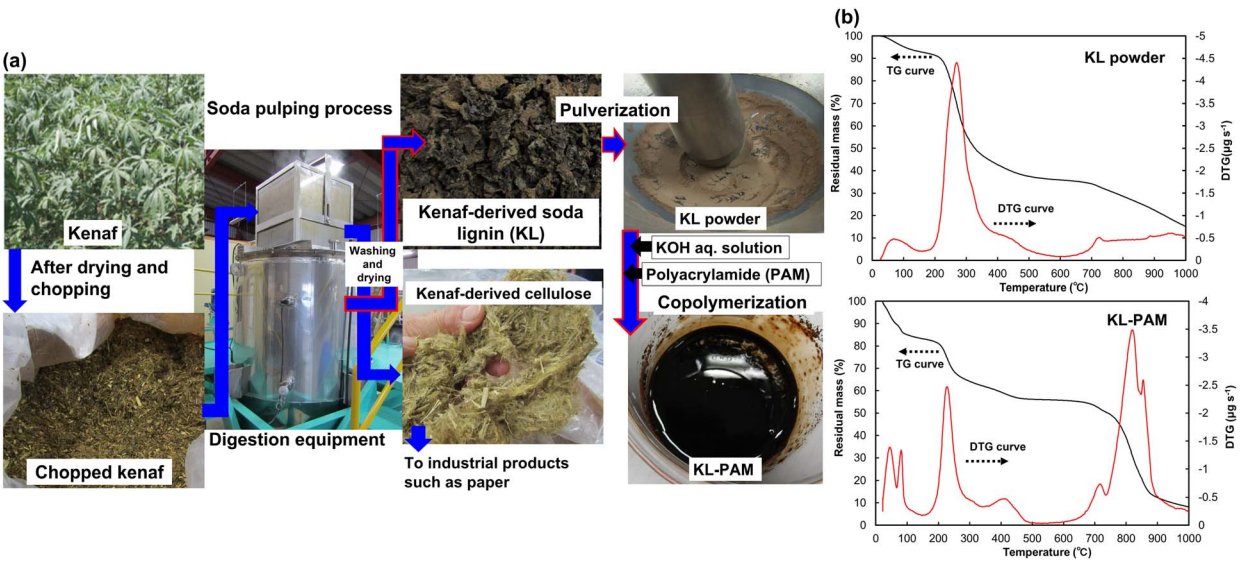

Fig. 1 (a) Process for producing KL-PAM from kenaf. (b) TG and DTG curves of KL powder and KL-PAM obtained from thermal analysis.

These peaks are attributed to partial decomposition of polymer chains in the copolymer (223–313 °C) and decomposition of the copolymer backbone (313–507 °C), respectively.[33] The residual mass of KL-PAM at 600 °C reaches 55.7%, which is 19.8% higher than that of KL. Plant-derived components are thermally decomposed and carbonized at temperatures up to approximately 600 °C. During this carbonization process, thermal decomposition and volatilization lead to mass loss. The difference in residual mass at 600 °C between KL and KL-PAM reflects their structural differences and indicates that KL-PAM is less prone to thermal decomposition and volatilization than KL. Also, considering that pristine PAM exhibits a residual mass of only 8.9% at 600 °C (Fig. S1), this result clearly indicates that copolymerization enhances the thermal stability of KL-PAM. In addition, the differences observed in the DTG curves of KL and KL-PAM above 700 °C suggest the formation of different carbonized residues.

Based on the thermal analysis of KL-PAM, the heat-treatment temperatures for electrode fabrication were set to 200, 400, 600, and 800 °C. The electrode slurry was prepared using deionized water as the solvent, with a composition of 80 wt% Si as the active material, 5 wt% carbon black (CK), and 15 wt% KL-PAM. The slurry was coated onto copper foil and subsequently heat-treated under an inert gas atmosphere at the designated temperatures. To clearly isolate and evaluate the binder performance, micron-sized Si particles were intentionally used, despite the common use of nano-Si or Si composites[1,5] to alleviate volume expansion effects. The obtained electrodes were designated as KL-PAM-*x*, where *x* corresponds to the first digit of the applied heat-treatment temperature. The surface morphology of the electrodes observed by scanning electron microscopy (SEM) is shown in Fig. 2(a). The surface morphology of KL-PAM-2 was similar to that of the electrode using PVDF as the binder (PVDF: 80 wt% Si, 5 wt% CK, 15 wt% PVDF; heat-treated at 160 °C, Fig. S2(d)), exhibiting a relatively flat surface. In KL-PAM-4, -6, and -8, circular depressions appeared on the electrode surfaces, with both their number and size increasing as the heat-treatment temperature rose. These features are attributed to the gasification reactions associated with the thermal decomposition of KL-PAM, suggesting that the extent of gasification increases at higher temperatures. In addition, small cracks were observed on the surface of KL-PAM-4 electrodes, and both the visibility and number of cracks increased with higher heat-treatment temperatures. These cracks are attributed to the shrinkage of electrode materials during thermal contraction, indicating that the effect of thermal shrinkage becomes more pronounced at elevated temperatures. Linear deposits observed along the edges of the

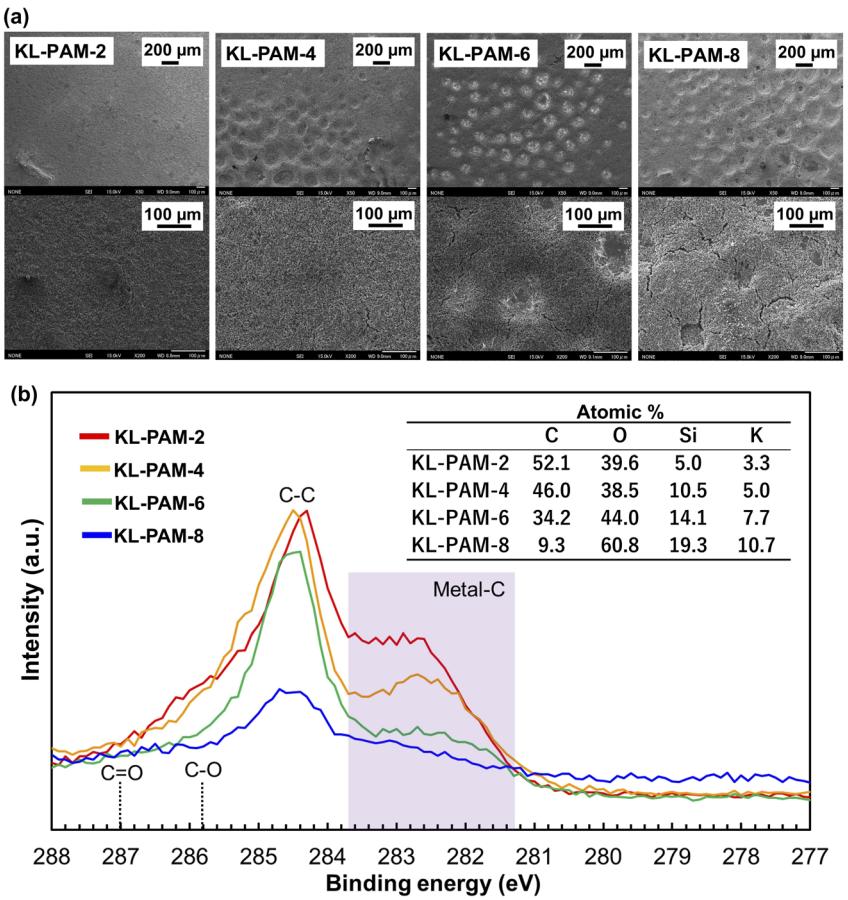

Fig. 2 (a) SEM images of the electrode surface of KL-PAM-*x* (*x*: the first digit of heat-treatment temperature of 200, 400, 600 or 800 °C), top high magnification, bottom low magnification. (b) Composition ratios and C 1s narrow scan spectra of KL-PAM-*x* obtained by XPS.

circular depressions in KL-PAM-6 (Fig. S2a) disappeared in KL-PAM-8 (Fig. S2b). This observation is consistent with the thermal analysis of KL-PAM and indicates that these deposits are residual carbonized products derived from KL-PAM. The residual carbonized deposits and the circular depressions observed at high heat-treatment temperatures were mitigated by incorporating CMC into the electrode slurry (KL-PAM-CMC-6; 75 wt% Si, 5 wt% CK, 15 wt% KL-PAM, and 5 wt% CMC; heat-treated at 600 °C), as shown in Fig. S2(c). This improvement is attributed to the dispersing effect of CMC,[7,8] which promotes a more uniform distribution of KL-PAM within the electrode material.

The surface composition of the electrodes was analyzed using X-ray photoelectron spectroscopy (XPS). The elemental ratios derived from the XPS survey spectra (Fig. S3) are presented in Fig. 2(b). To reflect the actual electrode fabrication conditions, no sputtering was applied in the XPS analysis. The carbon content decreased with increasing heat-treatment temperature, showing a sharp drop in KL-PAM-8. The narrow-scan XPS spectra of C 1s for the electrode surfaces are shown in Fig. 2(b). The peaks observed between 284 and 285 eV correspond to the relative contributions of sp^2 (C=C, 284 eV) and sp^3 (C–C, 285 eV) carbon,[45] with the main peak primarily attributed to aromatic C–C bonds.[46] Peaks corresponding to C–H, C–O, and C=O bonds appear at 284.1, 285.8, and 287.0 eV, respectively.[47,48] Bands associated with metal–carbon (metal–C) interactions are observed at lower binding energies than that of the C–C peak.[49] In KL-PAM-2 and -4, a broad band observed between 281.3 eV and 283.7 eV corresponds to the potassium–carbon combination band. The O 1s spectra (Fig. S4) showed a single large hump, with peak positions at 530.3 eV for KL-PAM-2 and -4, 530.8 eV for KL-PAM-6, and 530.1 eV for KL-PAM-8. In the O 1s spectra, the C–O and C=O bonding peaks appear at 531.2 eV and 532.1 eV, respectively.[47] Previous studies have reported that KOH-related species, including KOH, K^+–O, inorganic compound KOH, and organic compound KOH, exhibit binding energies lower than those of C–O and C=O, at 529.4, 530.0, 531.9, and 529.0 eV, respectively.[50–52] Therefore, the main peaks in the O 1s spectra are attributed to potassium species. Up to a heat-treatment temperature of 400 °C, the peaks correspond to a combination of KOH and organic compound KOH. At 600 °C, the organic compound KOH contribution becomes dominant, while at 800 °C, bands corresponding to K^+–O and inorganic compound KOH are more pronounced. This interpretation is further supported by the K 2p spectra (Fig. S4), where the two characteristic peaks, corresponding to K $2p_{1/2}$ and K $2p_{3/2}$, are shifted from their standard positions at 295.3 and 292.5 eV,[53] indicating the presence of potassium in complex chemical states. In KL-PAM-8, the potassium contained in KL-PAM is suggested to react with carbon at high temperatures, promoting carbon gasification and ultimately leaving inorganic potassium within the electrode. This process corresponds to the observed decrease in the spectral intensity between 281.3 and 283.7 eV at heat-treatment temperatures above 400 °C. In addition, it has been reported that the potassium activation reaction can generate CO_3^{2-} species (290.5 eV).[51] In the K 2p spectra of KL-PAM-8, the lower-energy peak is shifted further to lower binding energy, which can be attributed to the presence of the CO_3^{2-} band. Potassium activation is a common method for producing porous carbon, typically carried out at 800–900 °C.[54] The sharp decrease in carbon content observed in KL-PAM-8 can be attributed to carbon gasification induced by potassium activation, leading to the loss of the carbonized material. From the Si 2p spectra (Fig. S4), the surface of the Si particles was found to contain Si–OH functional groups (100.7 eV; O 1s: 532.3 eV).[55] As the heat-treatment temperature increased, these functional groups were removed, giving rise to Si–O–Si species (101.6 eV; O 1s: 531.6 eV).[52] In KL-PAM-8, a peak including Si–Si bonds (99.4 eV) appeared. These results suggest that high-temperature heat treatment may effectively remove functional groups generated on the active material particles during processing in aqueous slurries.

A rate test was conducted using the fabricated electrodes in half-cells. $LiPF_6$ in EC/DEC was used as the electrolyte, and the cell voltage was between 0 and 1 V at current densities of 0.1, 1, 5, and 10 mA cm^{-2}, with four cycles performed at each current density. The relationships between the electrode potential and the specific capacity for the first cycle and the last cycle at each current density, as obtained from the rate tests are shown in Fig. 3(a). Here, "extraction specific capacity" refers to the specific capacity corresponding to Li-ion extraction from the Si electrode (*i.e.*, the charging process in the half-cell configuration), whereas "insertion specific capacity" refers to the specific capacity associated with Li-ion insertion into the Si electrode (*i.e.*, the discharging process). PVDF and KL-PAM-CMC-6 are shown in Fig. S5. In Si-based anodes, the first lithiation not only forms a solid-electrolyte interphase (SEI) on the electrode surface, but also leads to repeated SEI formation due to the emergence of new surfaces associated with Si volume expansion. As a result, the initial Coulombic efficiency (ICE) is low. The ICEs of KL-PAM electrodes were 57.24% for KL-PAM-2, 40.84% for KL-PAM-4, 71.20% for KL-PAM-6, and 47.01% for KL-PAM-8. A Si electrode exhibiting a low ICE suggests that significant new interfaces were generated on the electrode surface due to the volume expansion of Si. In contrast, an electrode showing a high ICE indicates that the formation of new interfaces was suppressed. Namely, in this comparative study, KL-PAM-6 demonstrates higher mechanical strength than the other electrodes. The extraction specific capacities in the fourth cycle for KL-PAM-4 and -8 were 36.35% and 38.18% of their respective first-cycle extraction specific capacities, indicating that the electrode structures of KL-PAM-4 and -8 collapsed due to the volume expansion of Si during the initial lithiation. A similar trend was also observed for electrodes using PVDF as the binder (Fig. S5). Even after 20 cycles, KL-PAM-2 and -6 electrodes retained the plateau region at 0.43 V *vs.* Li/Li^+, indicating that rapid electrode collapse was suppressed. Although KL-PAM-2 exhibited a low ICE, indicating the formation of new surfaces due to Si volume expansion, the KL-PAM binder effectively prevented electrode structure collapse. In contrast, KL-PAM-6 showed a higher ICE, suggesting suppression of repeated SEI formation. This indicates that the electrode hardening induced by KL-PAM carbonization effectively stabilized the electrode structure. The rate capability of KL-PAM-

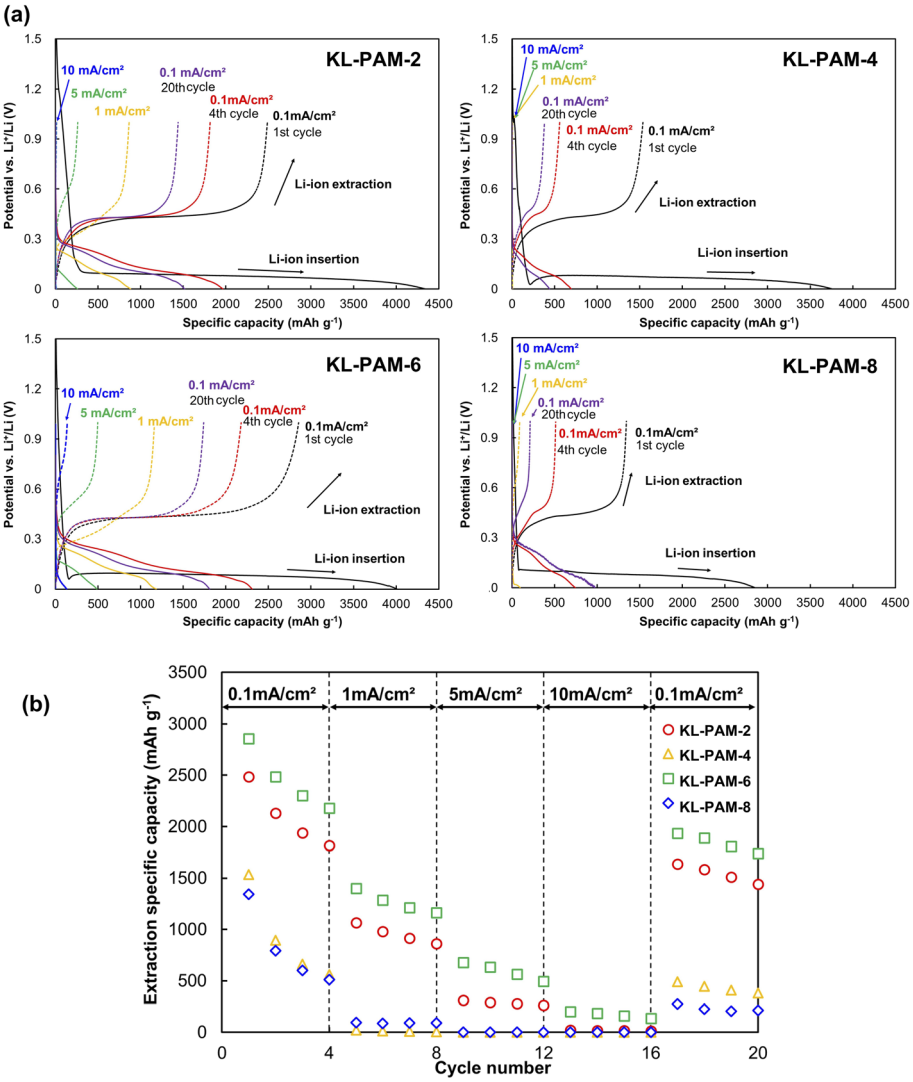

Fig. 3 (a) Relationship between the potential and specific capacity of KL-PAM-*x* electrodes during Li-ion insertion and extraction, as obtained from rate capability tests. (b) Comparison of KL-PAM-*x* rate performance (extraction specific capacity). (*x* indicates the first digit of heat-treatment temperature of 200, 400, 600 or 800 °C).

CMC-6 was slightly inferior to that of KL-PAM-6, indicating that material homogenization does not necessarily improve performance (Fig. S5). The extraction specific capacity obtained from the rate tests is shown in Fig. 3(b) (detailed data in Fig. S6). At the high rate (10 mA cm^{-2}), the difference in specific capacity among the cells became minimal due to the voltage drop caused by their internal resistance. However, KL-PAM-6 slightly retained its capacity. This suggests that the electronically conductive network formed through the carbonization of KL-PAM contributed to reducing the electrode resistance. The reversible extraction specific capacities of KL-PAM-2 and KL-PAM-6 after 20 cycles were 1440 and 1741 mAh g^{-1}, respectively. In contrast, the PVDF electrode showed a reversible specific capacity of only 58 mAh g^{-1}, indicating structural collapse during rate testing.

After the rate tests, a cycle test was conducted at a current density of 1 mA cm^{-2} within a voltage range of 0–1 V. KL-PAM-8 and PVDF electrodes, which exhibited severe capacity loss during the rate tests, were excluded from further testing. The cycling performance of KL-PAM-2 and -6 electrodes is shown in Fig. 4. The cycling results of KL-PAM-4 and KL-PAM-CMC-6 are presented in Fig. S7. The Coulombic efficiencies of KL-PAM-2 and -6 remained above 98% throughout the cycles after the initial cycle. Although KL-PAM-6 exhibited higher specific capacity during cycling compared to KL-PAM-2, both KL-PAM-2 and -6 showed a gradual capacity decline with repeated charge–discharge cycles. The extraction specific capacity retention relative to the first cycle for KL-PAM-2 and -6 was 54.7% (451 mAh g^{-1}) and 57.82% (637 mAh g^{-1}) after 50 cycles, and 32.7% (270 mAh g^{-1}) and 38.8% (427 mAh g^{-1}) after 100 cycles, respectively. The flexibility of KL-PAM to accommodate mechanical stress during Li-ion insertion and extraction, and the ability of KL-PAM carbonization to harden the electrode and prevent structural collapse, were found to have comparable

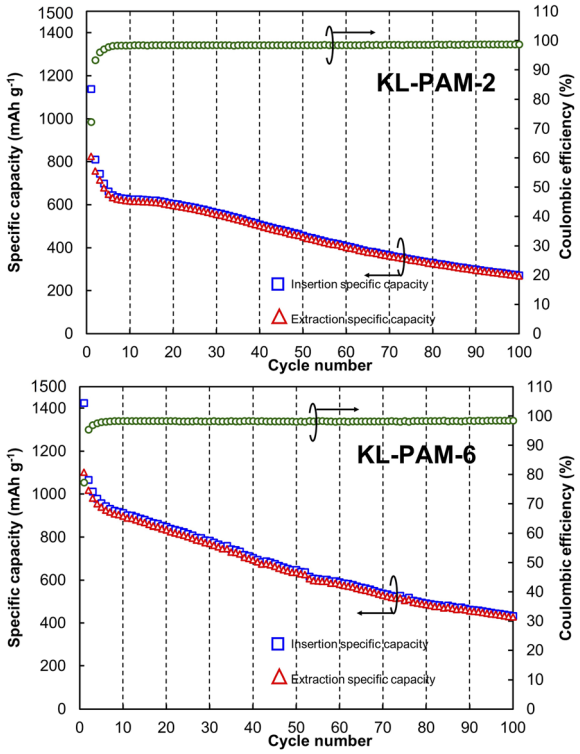

Fig. 4 Insertion and extraction specific capacities and coulombic efficiency during cycle testing of KL-PAM-2 and -6.

effects on cycling performance. KL-PAM-CMC-6 exhibited lower specific capacity and capacity retention than KL-PAM-2, indicating that material homogenization slightly deteriorated the cycling performance.

Conclusions

KL-PAM was developed as an aqueous binder for Si electrodes, and its thermally controlled dual stabilization mechanisms were clarified. Low-temperature heat treatment stabilized Si electrodes by exploiting the intrinsic flexibility and adhesion of KL-PAM to accommodate the large volume expansion of Si, whereas high-temperature heat treatment stabilized the electrodes through carbonization-induced hardening of KL-PAM, simultaneously enhancing electronic conductivity. Consequently, high-temperature-treated electrodes exhibited superior rate performance, while capacity retention was comparable between low- and high-temperature-treated electrodes. In both regimes, KL-PAM outperformed conventional binders as a Si electrode binder. Thermal treatment at intermediate temperatures was ineffective, as it activated neither sufficient flexibility nor carbonization-induced reinforcement, leading to binder failure. Moreover, high-temperature heat treatment introduced challenges such as surface cracking and alkali-metal-induced activation reactions, which caused gasification of carbonized structures and loss of binder functionality. In industrial electrode manufacturing, the heat treatment investigated in this study corresponds to the final thermal treatment step applied after drying the electrode sheets and cutting them into individual electrodes.[56] Since conventional vacuum heating equipment typically operates at temperatures up to approximately 300 °C, implementing a 600 °C process would require modification of the production line; however, such modification is technically feasible. Although high-temperature treatment provides improved rate capability at the expense of increased manufacturing cost, low-temperature treatment offers a cost-effective alternative. Therefore, both low- and high-temperature thermal treatment strategies are viable for lignin-based binders for Si electrodes, with distinct development pathways required according to their fundamentally different stabilization mechanisms.

Author contributions

Tatsuki Hozumi: methodology, investigation, formal analysis, data curation, writing – original draft. Reiichi Chiba: thermal analysis methodology, TG/DTA data investigation. Masanori Ikeda: XPS methodology, XPS data investigation. Daisuke Tashima: KL extraction methodology, writing – review & editing. Yusuke Abe: SEM methodology, data investigation. Seiji Kumagai: funding acquisition, conceptualization, methodology, supervision, writing – original draft, review & editing. Takuya Eguchi: funding acquisition, conceptualization, methodology, investigation, formal analysis, data curation, writing – original draft, review & editing.

Conflicts of interest

The authors declare no competing interests.

Data availability

Additional data can be obtained from the corresponding authors upon reasonable request.

The data supporting the findings of this study are available in the supplementary information (SI). Supplementary information is available. See DOI: https://doi.org/10.1039/d6se00053c.

Acknowledgements

This study was supported in part by Nihon University College of Engineering Grant, Nihon University SDG Project (grant number 24SDG02) and JSPS KAKENHI (grant numbers 23K13319 and 25H00726).

Notes and references

1 M. Je, D.-Y. Han, J. Ryu and S. Park, *Acc. Chem. Res.*, 2023, **56**, 2213–2224, DOI: 10.1021/acs.accounts.3c00308.
2 L. Yang, T. Meng, W. Zheng, J. Zhong, H. Cheng, Y. Tong and D. Shu, *Energy Storage Mater.*, 2024, **72**, 103766, DOI: 10.1016/j.ensm.2024.103766.
3 T. Cai, W. Wahyudi, P. Kumar, Z. Ma, Q. Sun, H. Xie, Y. Wang, F. Zhao, Z. Cao, L. Cavallo, Q. Li and J. Ming,

Mater. Sci. Eng., R, 2024, **161**, 100854, DOI: 10.1016/j.mser.2024.100854.
4 S. V. Gopinadh, P. V. R. L. Phanendra, A. V. Anoopkumar, B. John and M. T. D. Mercy, *Energy Fuels*, 2024, **38**, 17253–17277, DOI: 10.1021/acs.energyfuels.4c03023.
5 J. Zhang, Y. Zhai, Z. Zhao, J. He, W. Wei, J. Xiao, S. Wu and Q.-H. Yang, *Acta Phys. Chim. Sin.*, 2024, **40**, 2306006, DOI: 10.3866/PKU.WHXB202306006.
6 N. A. Salleh, S. Kheawhom, N. A. A. Hamid, W. Rahiman and A. A. Mohamad, *J. Mater. Res. Technol.*, 2023, **23**, 3470–3491, DOI: 10.1016/j.jmrt.2023.02.013.
7 H. Chen, M. Ling, L. Hencz, H. Y. Ling, G. Li, Z. Lin, G. Liu and S. Zhang, *Chem. Rev.*, 2018, **118**, 8936–8982, DOI: 10.1021/acs.chemrev.8b00241.
8 Q. He, J. Ning, H. Chen, Z. Jiang, J. Wang, D. Chen, C. Zhao, Z. Liu, I. F. Perepichka, H. Meng and W. Huang, *Chem. Soc. Rev.*, 2024, **53**, 7091–7157, DOI: 10.1039/d4cs00366g.
9 A. N. Preman, H. Lee, J. Yoo, I. T. Kim, T. Saito and S. Ahn, *J. Mater. Chem. A*, 2020, **8**, 25548–25570, DOI: 10.1039/d0ta07713e.
10 O. Mukhan, J.-S. Yun, E. K. Kim, S.-G. Ji, N. Umirov, B.-M. Lee, C.-U. Jeong, S.-S. Kim and J.-H. Choi, *Polymer*, 2023, **280**, 126042, DOI: 10.1016/j.polymer.2023.126042.
11 H. S. Yang, S.-H. Kim, A. G. Kannan, S. K. Kim, C. Park and D.-W. Kim, *Langmuir*, 2016, **32**, 3300–3307, DOI: 10.1021/acs.langmuir.6b00205.
12 Z. Li, Y. Zhang, T. Liu, X. Gao, S. Li, M. Ling, C. Liang, J. Zheng and Z. Lin, *Adv. Energy Mater.*, 2020, **10**, 1903110, DOI: 10.1002/aenm.201903110.
13 Y. Kang, N. Dong, F. Liu, D. Lin, B. Liu, G. Tian, S. Qi and D. Wu, *J. Energy Chem.*, 2024, **93**, 580–591, DOI: 10.1016/j.jechem.2024.02.031.
14 J. Liu, Q. Zhang, T. Zhang, J.-T. Li, L. Huang and S.-G. Sun, *Adv. Funct. Mater.*, 2015, **25**, 3599–3605, DOI: 10.1002/adfm.201500589.
15 T. Munaoka, X. Yan, J. Lopez, J. W. F. To, J. Park, J. B.-H. Tok, Y. Cui and Z. Bao, *Adv. Energy Mater.*, 2018, **8**, 1703138, DOI: 10.1002/aenm.201703138.
16 Y. Kang, M. Lee, D. Ji, J. Bae, C. Lee and W. Lee, *Chem. Commun.*, 2025, **61**, 14418–14421, DOI: 10.1039/d5cc02197a.
17 J. Liu, Q. Zhang, Z.-Y. Wu, J.-H. Wu, J.-T. Li, L. Huang and S.-G. Sun, *Chem. Commun.*, 2014, **50**, 6386–6389, DOI: 10.1039/c4cc00081a.
18 A. Samridh, S. V. Gopinadh, B. John, S. Sarojiniamma, M. T. Devassia and M. G. Joseph, *Energy Technol.*, 2025, **13**, 2401837, DOI: 10.1002/ente.202401837.
19 A. Samridh, S. V. Gopinadh, B. John, P. V. R. L. Phanindra, J. M. Gladis, S. Sujatha and T. D. Mercy, *RSC Sustainability*, 2025, **3**, 5333–5345, DOI: 10.1039/d5su00186b.
20 M. Mili, S. A. R. Hashmi, M. Ather, V. Hada, N. Markandeya, S. Kamble, M. Mohapatra, S. K. S. Rathore, A. K. Srivastava and S. Verma, *J. Appl. Polym. Sci.*, 2022, **139**, e51951, DOI: 10.1002/app.51951.
21 T. C. Nirmale, B. B. Kale and A. J. Varma, *Int. J. Biol. Macromol.*, 2017, **103**, 1032–1043, DOI: 10.1016/j.ijbiomac.2017.05.155.
22 J. Domínguez-Robles, R. Sánchez, P. Díaz-Carrasco, E. Espinosa, M. T. García-Domínguez and A. Rodríguez, *Int. J. Biol. Macromol.*, 2017, **104**, 909–918, DOI: 10.1016/j.ijbiomac.2017.07.015.
23 H. Lu, A. Cornell, F. Alvarado, M. Behm, S. Leijonmarck, J. Li, P. Tomani and G. Lindbergh, *Materials*, 2016, **9**, 127, DOI: 10.3390/ma9030127.
24 C. Luo, L. Du, W. Wu, H. Xu, G. Zhang, S. Li, C. Wang, Z. Lu and Y. Deng, *ACS Sustain. Chem. Eng.*, 2018, **6**, 12621–12629, DOI: 10.1021/acssuschemeng.8b01161.
25 P. Khamnantha, C. Homla-or, K. Suttisintong, J. Manyam, M. Raita, V. Champreda, V. Intasanta, H.-J. Butt, R. Berger and A. Pangon, *ACS Appl. Nano Mater.*, 2021, **4**, 13099, DOI: 10.1021/acsanm.1c02637.
26 J.-M. Yuan, W.-F. Ren, K. Wang, T.-T. Su, G.-J. Jiao, C.-Y. Shao, L.-P. Xiao and R.-C. Sun, *ACS Sustain. Chem. Eng.*, 2022, **10**, 166, DOI: 10.1021/acssuschemeng.1c05359.
27 Z. Chen, M. Lu, Y. Qian, Y. Yang, J. Liu, Z. Lin, D. Yang, J. Lu and X. Qiu, *Adv. Energy Mater.*, 2023, **13**, 2300092, DOI: 10.1002/aenm.202300092.
28 D. Jeong, J. Shim, H. Shin and J.-C. Lee, *ChemSusChem*, 2020, **13**, 2642–2649, DOI: 10.1002/cssc.201903466.
29 T. Chen, Q. Zhang, J. Xu, J. Pan and Y.-T. Cheng, *RSC Adv.*, 2016, **6**, 29308–29313, DOI: 10.1039/c6ra03001g.
30 T. Chen, Q. Zhang, J. Pan, J. Xu, Y. Liu, M. Al-Shroofy and Y.-T. Cheng, *ACS Appl. Mater. Interfaces*, 2016, **8**, 32341–32348, DOI: 10.1021/acsami.6b11500.
31 Q. Yao, J. Xie, J. Liu, H. Kang and Y. Liu, *J. Polym. Res.*, 2014, **21**, 465, DOI: 10.1007/s10965-014-0465-9.
32 C. Gao, X. Wang, S. Zhai and Q. An, *Int. J. Biol. Macromol.*, 2019, **134**, 202, DOI: 10.1016/j.ijbiomac.2019.05.017.
33 S. Wang, Y. Sun, F. Kong, G. Yang and P. Fatehi, *BioResources*, 2016, **11**, 1765–1783, DOI: 10.15376/biores.11.1.1765-1783.
34 K. Wang, J. Qiu, W. Huang, Z. Yuan, B. Wei and Y. Wen, *Int. J. Biol. Macromol.*, 2025, **296**, 139730, DOI: 10.1016/j.ijbiomac.2025.139730.
35 C. Chen, N. Zheng, W. Wu, M. Tang, W. Feng, W. Zhang, X. Li, Y. Jiang, J. Pang, D. Min and L. Fu, *ACS Appl. Mater. Interfaces*, 2022, **14**, 54127–54140, DOI: 10.1021/acsami.2c12914.
36 A. Hasan and P. Fatehi, *Colloids Surf., A*, 2019, **572**, 230–236, DOI: 10.1016/j.colsurfa.2019.04.002.
37 A. Hasan and P. Fatehi, *Appl. Clay Sci.*, 2018, **158**, 72–82, DOI: 10.1016/j.clay.2018.02.048.
38 M. Pourmahdi, M. Mohsenpour and M. Abdollahi, *Wood Sci. Technol.*, 2023, **57**, 1099–1123, DOI: 10.1007/s00226-023-01485-3.
39 K. Ji, R. Li, H. Zhou, M. Xia and F. Sun, *Polym. Bull.*, 2025, **82**, 9125–9147, DOI: 10.1007/s00289-025-05878-1.
40 T. B. T. Lam, K. Hori and K. Iiyama, *J. Wood Sci.*, 2003, **49**, 255–261, DOI: 10.1007/s10086-002-0469-7.
41 A.-G. N. Abbas, F. N. A. A. Aziz, K. Abdan, N. A. Mohd Nasir and M. N. Norizan, *Fibers*, 2022, **10**, 3, DOI: 10.3390/fib10010003.

42 T. Eguchi, T. Naganuma, R. Chiba, K. Watanabe, Y. Abe and S. Kumagai, *Int. J. Soc. Mater. Eng. Resour.*, 2024, **27**, 663, DOI: 10.5188/ijsmer.663.
43 E. Melro, A. Filipe, D. Sousa, A. J. M. Valente, A. Romano, F. E. Antunes and B. Medronho, *Int. J. Biol. Macromol.*, 2020, **148**, 688–695, DOI: 10.1016/j.ijbiomac.2020.01.153.
44 A. Meraj, M. Jawaid, S. P. Singh, M. M. Nasef, H. Ariffin, H. Fouad and B. Abu-Jdayil, *Sci. Rep.*, 2024, **14**, 8672, DOI: 10.1038/s41598-024-59200-6.
45 D. Ristiani, R. Asih, F. Astuti, M. A. Baqiya, C. Kaewhan, S. Tunmee, H. Nakajima, S. Soontaranon and D. Darminto, *Heliyon*, 2022, **8**, e09032, DOI: 10.1016/j.heliyon.2022.e09032.
46 J. A. Donadelli, A. Cánneva, G. Erra and A. Calvo, *Fuel*, 2019, **257**, 116004, DOI: 10.1016/j.fuel.2019.116004.
47 H. Xu, Q. Wang, H. Xiao, X. Li, X. Su, M. Tang, L. Chen and S. Li, *RSC Adv.*, 2019, **9**, 1319–1326, DOI: 10.1039/c8ra09095e.
48 T.-G. Woo, I.-S. Park, K.-H. Jung, W.-Y. Jeon and K.-W. Seol, *Met. Mater. Int.*, 2011, **17**, 789–795, DOI: 10.1007/s12540-011-1015-1.
49 A. Roy, A. K. Mukhopadhyay, S. C. Das, G. Bhattacharjee, A. Majumdar and R. Hippler, *Coatings*, 2019, **9**, 551, DOI: 10.3390/coatings9090551.
50 L. Caracciolo, L. Madec and H. Martinez, *ACS Appl. Energy Mater.*, 2021, **4**, 11693–11699, DOI: 10.1021/acsaem.1c02400.
51 B. Dziejarski, J. Serafin, D. F. Hernández-Barreto, E. Naumovska, J. Srénscek-Nazzal, N. Klomkliang, E. Tam, R. Krzyżyńska, K. Andersson and P. Knutsson, *Chem. Eng. J.*, 2025, **524**, 169677, DOI: 10.1016/j.cej.2025.169677.
52 M.-E. Yvenat, B. Chavillon, E. Mayousse, E. De Vito, A. Boulineau, F. Perdu and P. Azaïs, *Sustainable Energy Fuels*, 2023, **7**, 4150–4159, DOI: 10.1039/d3se00594a.
53 Z. Shen, X. Xing, S. Wang, M. Lv, J. Li and T. Li, *ACS Omega*, 2022, **7**, 8798–8807, DOI: 10.1021/acsomega.1c07076.
54 T. Eguchi, D. Tashima, M. Fukuma and S. Kumagai, *J. Cleaner Prod.*, 2020, **259**, 120822, DOI: 10.1016/j.jclepro.2020.120822.
55 R. Huang, M. Tang, W. Kan, H. Xu, K. Wu, Z. Wang and H. Li, *J. Phys. D: Appl. Phys.*, 2024, **57**, 015102, DOI: 10.1088/1361-6463/acff05.
56 J. Li, J. Fleetwood, W. B. Hawley and W. Kays, *Chem. Rev.*, 2022, **122**, 903–956, DOI: 10.1021/acs.chemrev.1c00565.

